

# Dynamically-downscaled projections of changes in temperature extremes over China

Junhong Guo<sup>1</sup> · Guohe Huang<sup>2,3</sup> · Xiuquan Wang<sup>2,4</sup> · Yongping Li<sup>5</sup> · Qianguo Lin<sup>1</sup>

Received: 8 January 2017 / Accepted: 21 March 2017 / Published online: 8 June 2017  
© Springer-Verlag Berlin Heidelberg 2017

**Abstract** In this study, likely changes in extreme temperatures (including 16 indices) over China in response to global warming throughout the twenty-first century are investigated through the PRECIS regional climate modeling system. The PRECIS experiment is conducted at a spatial resolution of 25 km and is driven by a perturbed-physics ensemble to reflect spatial variations and model uncertainties. Simulations of present climate (1961–1990) are compared with observations to validate the model performance in reproducing historical climate over China. Results indicate that the PRECIS demonstrates reasonable skills in reproducing the spatial patterns of observed extreme temperatures over the most regions of China, especially in the east. Nevertheless, the PRECIS shows a relatively poor performance in simulating the spatial patterns of extreme temperatures in the western mountainous regions, where its driving GCM exhibits more uncertainties due to

lack of insufficient observations and results in more errors in climate downscaling. Future spatio-temporal changes of extreme temperature indices are then analyzed for three successive periods (i.e., 2020s, 2050s and 2080s). The projected changes in extreme temperatures by PRECIS are well consistent with the results of the major global climate models in both spatial and temporal patterns. Furthermore, the PRECIS demonstrates a distinct superiority in providing more detailed spatial information of extreme indices. In general, all extreme indices show similar changes in spatial pattern: large changes are projected in the north while small changes are projected in the south. In contrast, the temporal patterns for all indices vary differently over future periods: the warm indices, such as SU, TR, WSDI, TX90p, TN90p and GSL are likely to increase, while the cold indices, such as ID, FD, CSDI, TX10p and TN10p, are likely to decrease with time in response to global warming. Nevertheless, the magnitudes of changes in all indices tend to decrease gradually with time, indicating the projected warming will begin to slow down in the late of this century. In addition, the projected range of changes for all indices would become larger with time, suggesting more uncertainties would be involved in long-term climate projections.

✉ Guohe Huang  
huang@iseis.org

✉ Xiuquan Wang  
xiuquan.wang@gmail.com

<sup>1</sup> Key Laboratory of Regional Energy and Environmental Systems Optimization, Ministry of Education, North China Electric Power University, Beijing 102206, China

<sup>2</sup> Institute for Energy, Environment and Sustainable Communities, University of Regina, 3737 Wascana Parkway, Regina, SK S4S 0A2, Canada

<sup>3</sup> SC Institute for Energy, Environment and Sustainability Research, North China Electric Power University, Beijing 102206, China

<sup>4</sup> Department of Civil and Resource Engineering, Dalhousie University, Halifax, NS B3H 4R2, Canada

<sup>5</sup> School of Environment, Beijing Normal University, Beijing 100875, China

**Keywords** Extreme temperature indices · High resolution · Regional climate model · Climate change · China

## 1 Introduction

Global warming resulted from increased greenhouse gases in the atmosphere has attracted increasing attention due to its close correlation with natural disasters (Hartmann et al. 2014; Meinshausen et al. 2009). Over the past century,

the frequency and magnitude of natural disasters, such as droughts, floods, tropical cyclones and sand storms, have shown an increasing trend over the world. This has become a common and daunting challenge facing humankind, as it often leads to devastating consequences (Diaz 2007; Etterson and Shaw 2001; Meinshausen et al. 2009; Root et al. 2003). Moreover, many studies have suggested that the global warming tends to increase in the future, with the global average surface temperature rising 0.3–0.48 °C by the end of this century (Hartmann et al. 2014). Thus, it is important to forecast future climate change at regional and local scales to support the assessment of the potential impacts of climate extremes, and provide scientific basis for developing appropriate adaptation and mitigation measures. Among many extreme climate events, heat waves and cold spells are two typical temperature extreme events of particular interest as they often have significant negative effects on human communities, agroecosystems, and the socio-economic development. Projection of potential changes in temperature extreme events and development of effective adaptation strategies are therefore necessary and urgent for policy makers and resources managers.

Nowadays, many studies on temperature extremes have been reported in different regions of the world, such as America (Filahi et al. 2016; Grotjahn et al. 2016; Marengo et al. 2009; Schoof and Robeson 2015), European (Beniston et al. 2007; Cardil et al. 2014; Déqué 2007; Fioravanti et al. 2016), Asia (Araghi et al. 2016; Iqbal et al. 2016; Karim and Rahman 2015; Mahmood et al. 2015), Africa (Mason et al. 1999; Panthou et al. 2012) etc. With regard to the research methodology, the traditional extreme value theory (EVT) based on the return periods or return values is used to simulate the tails of statistical distributions, especially better to investigate changes in unusual events to some extent. Nonetheless, the given climatic time series is analyzed on the basis of some critical assumptions that the intensity and frequency of extreme events should follow certain mathematical distribution (i.e., Gumbel, Fréchet or Weibull). On the other hand, alternative approaches are introduced by using threshold or percentile exceedances metrics. The world climate research programme (WCRP) project on expert team on climate change detection and indices (ETCCDI) has developed more intuitive indicators to interpret the extreme events easily. Due to its clear interpretation and easy employment, the ETCCDI indices have been widely accepted and used to compare climate extremes simulated from different climate models (Filahi et al. 2016; Fioravanti et al. 2016; Kim et al. 2015; Sun et al. 2016). The 16 core temperature extreme indices defined by the ETCCDI are described in Table 1. In this paper, we follow the classification method used by most studies (Jiang et al. 2015; Sun et al. 2016) classify these

indices into two groups for comparison purpose: warm indices and cold indices. As shown in Table 1, warm indices include number of summer days (SU), number of tropical nights (TR), warm days (TX90p), warm nights (TN90p), warm spell duration index (WSDI) and growing season length (GSL), while cold indices include number of icing days (ID), number of frost days (FD), cold days (TX10p), cold nights (TN10p) and cold spell duration index (CSDI).

Generally, station observations are often used to statistically investigate the temporal variation trend as the first real data of the past, and the arithmetic mean of values of all stations is usually used to represent the entire regional climate (Filahi et al. 2016; Fioravanti et al. 2016; Jiang et al. 2015). However, uneven station coverage and missing values could be the biggest shortcomings, which cannot reflect the reality of the entire region, especially in the remote areas or complex terrains. On the other hand, the outputs from climate models are also often used to analyze the future trends of climate extremes in a certain region. For example, the projections of global climate models (GCMs) are applied to evaluate the impact of climate change on the intensity and frequency of temperature extremes in different emission scenarios in previous studies (Beharry et al. 2015; Kitoh and Endo 2016). However, the coarse resolution of GCMs cannot be competent for simulations at regional and local scales, and even there are some biases at sub-continental regions. Through downscaling technologies, such as statistical downscaling and dynamical downscaling, deriving the changes in regional and local extremes at a higher spatial and temporal resolution is likely to compensate for the deficiencies of GCMs.

Statistical downscaling is conducted to build the historical quantitative relationships between large-scale coarse atmospheric variables (predictors) and local weather variables (predictands), and then apply these relationships to produce future climate data. Because of its easy to use, low computational expense and various options, statistical downscaling has been widely used by many researchers (Busuioc et al. 2001; Mahmood and Babel 2014; Timbal and Jones 2008; Wang et al. 2013). For statistical downscaling, the quality of the historical data determines the performance and robustness of simulation model and sometimes the established math-statistics mapping between predictors and predictands may not meet future situations due to the excessive dependence on the current climate factors. By contrast, with sharing similar physical processes and mechanisms as described in GCMs, dynamical downscaling nests fine-resolution regional climate models (RCMs) into GCMs, and the outputs downscaled by RCMs with finer-scale surface forcing can produce more local or regional detail information, so the results could be more credible. Given these benefits, we apply a dynamical

**Table 1** 16 ETCCDI extreme temperature indices

Category	Index	Descriptive name	Definitions	Units
Monthly extremal indices	TXx	Warmest day	Monthly maximum value of daily maximum temperature	°C
	TXn	Coldest day	Monthly minimum value of daily maximum temperature	°C
	TNx	Warmest night	Monthly maximum value of daily minimum temperature	°C
	TNn	Coldest night	Monthly minimum value of daily minimum temperature	°C
Absolute indices	ID	Number of icing days (–)	Annual count of days when TX (daily maximum temperature) <0 °C	Days
	FD	Number of frost days (–)	Annual count of days when TN (daily minimum temperature) <0 °C	Days
	SU	Number of summer days (+)	Annual count of days when TX (daily maximum temperature) >25 °C	Days
	TR	Number of tropical nights (+)	Annual count of days when TN (daily minimum temperature) >20 °C	Days
Relative indices	TX10p	Cold days (–)	Percentage of days when TX <10th percentile of 1961–1990	%days
	TX90p	Warm days (+)	Percentage of days when TX >90th percentile of 1961–1990	%days
	TN10p	Cold nights (–)	Percentage of days when TN <10th percentile of 1961–1990	%days
	TN90p	Warm nights (+)	Percentage of days when TN >90th percentile of 1961–1990	%days
Spell duration indices	WSDI	Warm spell duration index (+)	Annual count of days with at least 6 consecutive days when TX >90th percentile	Days
	CSDI	Cold spell duration index (–)	Annual count of days with at least 6 consecutive days when TN <10th percentile	Days
	GSL	Growing season length (+)	Annual count between first span of at least 6 days with daily mean temperature TG >5 °C and first span after July 1st of 6 days with TG <5 °C	Days
	DTR	Daily temperature range	Monthly mean difference between TX and TN	°C

These indices are divided into monthly extremal indices, absolute indices, relative indices and spell duration indices. The indices with plus sign are warm ones and with minus sign are cold ones

downscaling modeling system (PRECIS) in climate simulations and projections over China.

In China, the cold center is located in the north, whereas heat waves frequently occur in the southeast, and droughts often happen in arid and semi-arid areas of the northwest of China. With complex topography and unique climate systems, China is one of the countries that are often hit by extreme events, and the frequency and intensity of natural disasters are on the rise in recent years. For example, from 2009 to 2010 continuous severe droughts in most parts of southern Yunnan province caused considerable losses and threats to Chinese economy (LU et al. 2012; Qiu 2010). In the early summer of 2008, sudden temperature drop and snowstorms caused great damage to agricultural production in northern Hebei province.

Many scholars have engaged in temperature extremes studies in several typical climatic regions in China, such as hot south (Zhang et al. 2016b), cold northeast (Wang et al. 2016) and the southwest (Qin et al. 2015), main river basin, such as Poyang Lake basin (Zhang et al. 2016a), Yangtze River Basin (Guan et al. 2015) and Yellow River basin (Liang et al. 2014), and other special concerned regions, such as Qinling Mountains (Jiang et al. 2015) and Shijiazhuang station (Bian et al. 2015). Previous studies on

temperature extremes in China have shortcomings, such as small contained areas, low resolution, short period of time and more uncertainty. As an improvement to aforementioned studies, we investigate the possible changes in extreme temperatures (including 16 indices) over China in response to global warming through the PRECIS regional climate modeling system at 25-km spatial resolution. The performance of the model is validated by comparison with observation data in the baseline period (1961–1990). The future changes in the spatial and temporal patterns of temperature extremes across the country are analyzed afterwards.

## 2 Data and method

### 2.1 Observations and validation methods

The maximum and minimum daily temperature observations are obtained from the gridded climate dataset (SURF\_CLI\_CHN\_TEM\_DAY\_GRID\_0.5, V2.0), provided by National Meteorological Information Center (NMIC), China. The dataset is based on a large amount of national meteorological stations from 1961, and spatial interpolated

onto spatial grids with  $0.5^\circ \times 0.5^\circ$  horizontal resolution using a thin plate spline method and three-dimensional spatial information technology (see <http://data.cma.cn/>). Here, we extract the data from 1961 to 1990 to represent the observations of current climate in the context of China.

In order to quantify and compare the model's performance in simulating the indices from correlations and errors, we also calculated the Pearson sample linear cross-correlation coefficient (PLCC) and the Nash–Sutcliffe efficiency (NSE) between observations and the corresponding model simulations during the baseline period over the entire China.

$$PLCC = \frac{\sum (X - \bar{X})(Y - \bar{Y})}{N \left( \sqrt{\frac{1}{n} \sum_{i=1}^n (X_i - \bar{X})^2} \right) \left( \sqrt{\frac{1}{n} \sum_{i=1}^n (Y_i - \bar{Y})^2} \right)}, \quad (1)$$

$$NSE = 1 - \frac{\sum_{i=1}^n (X_i - Y_i)^2}{\sum_{i=1}^n (X_i - \bar{X})^2}, \quad (2)$$

where  $X_i$  and  $Y_i$  represent the observed and simulated values for each cell grid,  $\bar{X}$  and  $\bar{Y}$  represent the mean value of observation and simulation. Meanwhile, we follow a rating approach (Khan and Valeo 2016; Moriasi et al. 2007) to calculate the rank (i.e., 0, 0.33, 0.66 and 1) for each 16 indices, and then combine these ranks to give an “average rating” (AR) to evaluate the overall performance of PRECIS (Table 2).

## 2.2 Regional climate modeling and uncertainties

The providing regional climates for impacts studies (PRECIS) is a regional climate modelling system developed by the Met Office Hadley Centre. It has been widely used to simulate climate change, because of its easy-to-use and wide suitability for generating detailed climate change scenarios in any area of the globe (Buontempo et al. 2014; Wang et al. 2015a, b, 2014). As a high-resolution atmosphere and land surface regional climate model, PRECIS has 50 and 25-km resolutions at the equator of the rotated regular latitude-longitude grid and contains 19 levels in

the vertical. The GCM data used to drive PRECIS is provided by the Hadley Centre's global atmospheric-only model HadAM3P with a horizontal resolution of  $3.75^\circ$  longitude and  $2.5^\circ$  latitude to generate the regional model's lateral boundary conditions (LBCs), and the land surface model employs Met Office Surface Exchange Scheme 2.2 (MOSES 2.2) (Noguer et al. 2003).

In general, the uncertainties in climate modeling and climate change predictions include three aspects: (1) Emission scenario. The probabilities of future scenarios, whether SRES or RCPs, are not clear since there are inherent uncertainties in the key assumptions and relationships about future population, socio-economic development and technical changes. (2) Initial conditions. There are large differences in the same model and emission scenario, but with different initial conditions. (3) Model uncertainty. The climate system is complex so that all processes and parameters are uncertain in climate models.

These uncertainties influence our understanding towards climate change, which could lead to our incorrect or incomplete description of key processes and feedbacks in climate model. Although these uncertainties are inevitable, they can be quantified by running ensembles of future climate projections (Buontempo et al. 2014; Marengo et al. 2009; Murphy et al. 2004; Wang et al. 2015b). Two types of model ensemble generation methods are used to capture or quantify these uncertainties. The multi-model ensemble collects GCM output from different modelling centers around the world into a central repository (i.e., CMIP3 and CMIP5) to allow inter-model comparisons and analysis (Cheng et al. 2015; Pepler et al. 2015). This method provides the possibility to explore the uncertainty range of model, but the disagreements between models can be large at regional scales owing to using different structural choices in model formulation. An alternative route is called the “perturbed physics” approach by varying the values of the parameters in a single model to give the range of future outcomes. The advantage of perturbations is that variations in model formulation allow us to generate larger ensembles to explore nonlinearities and extreme behavior. It is also possible to clearly distinguish the effects of some prior assumptions by showing the sensitivity of the ensemble output by using different observational constraints and experimental designs (Collins et al. 2006).

PRECIS provides an ensemble of perturbed physics LBCs, based on the HadCM3 model of Met Office Hadley Center for quantifying uncertainty in model projections (hereinafter referred to as QUMP) under the IPCC SRES A1B emissions scenario. The QUMP ensemble consists of 17 members (HadCM3Q0–Q16) and each one has a set of perturbations to its unique dynamical and physical formulation, representing different boundary conditions and climate sensitivity (McSweeney et al. 2012). Specifically, HadCM3Q0 is a

**Table 2** Rating table used to quantify the overall model's performance

Average rating	Performance
$AR > 0.9$	Very good
$0.66 < AR \leq 0.9$	Good
$0.33 < AR \leq 0.66$	Satisfactory
$0.0 < AR \leq 0.33$	Unsatisfactory

basic, standard and unperturbed model that uses the original parameter settings as applied in the atmospheric component of HadCM3, and the other 16 members (Q1-Q16) make different changes in some climate parameters. However, if we entirely downscale the 17 members with PRECIS, it would be very expensive and requires a lot of computing resources, data storage and data analyses. In this study, in order to minimize the requirements while exploring a wide range of uncertainties, we selected Q0 (unperturbed), Q1 (low-sensitivity), Q7 (mid-sensitivity), Q10 (mid-sensitivity) and Q13 (high-sensitivity) from the ensemble of QUMP as LBCs to run the PRECIS model from 1950 to 2099 with a 25-km spatial resolution.

### 2.3 Trend and uncertainty analysis methods

As a non-parametric statistically evaluation, Mann–Kendall (MK) test is used in trend analysis on extremes, because the extreme data series cannot meet the Gaussian distribution (Hamed and Rao 1998; Salmi et al. 2002; Sang et al. 2014; Zhang et al. 2017). The MK test is based on the test statistic S:

$$S = \sum_{i=1}^{n-1} \sum_{j=i+1}^n \text{sgn}(x_j - x_i), \tag{3}$$

where  $x_j$  and  $x_i$  are two adjacent values in time series with the length of n for each grid, and the sign function is defined by:

$$\text{sgn}(\theta) = \begin{cases} 1, & \theta > 0 \\ 0, & \theta = 0 \\ -1, & \theta < 0 \end{cases} \tag{4}$$

A positive (negative) value of S indicates an upward (downward) trend. For time series with less than 10 data points, the S statistic is used; for time series with 10 or more data points, the S is approximately normally distributed, with the mean E(S) and variance Var(S) as follows:

$$E(S) = 0, \tag{5}$$

$$\text{Var}(S) = \frac{n(n-1)(2n+5) - \sum_{i=1}^p t_i(t_i-1)(2t_i+5)}{18}, \tag{6}$$

where  $t_i$  is the number of data in the tied group and p is the number of tied groups. The standardized test statistic Z follows the standard normal distribution:

$$Z = \begin{cases} \frac{S-1}{\sqrt{\text{var}(S)}}, & S > 0 \\ 0, & S = 0 \\ \frac{S+1}{\sqrt{\text{var}(S)}}, & S < 0 \end{cases} \tag{7}$$

The null hypothesis of no trend is accepted if the absolute value of Z is in the theoretical range between  $-Z_{1-\delta/2}$  and  $Z_{1-\delta/2}$ , where  $\delta$  is the statistical significance level concerned.

The magnitude of trends will be calculated by the Theil-Sen trend estimation method, which can be more accurate than simple linear regression for statistics of skewed distribution, and competes well against non-robust least squares even for normally distributed data on the basis of statistical power (Ahmed 2014; Fonseca et al. 2015). The magnitude of change is expressed as a percentage of the mean:

$$\beta = \text{median} \left( \frac{x_j - x_k}{j - k} \right), \quad j = 1, 2, \dots, n \quad k = 1, 2, \dots, j - 1, \tag{8}$$

where  $x_j$  and  $x_k$  are data values at times j and k ( $j > k$ ),  $\beta$  is the Theil-Sen’s estimator of slope.

To have a good characterization of probability projections, the interval analysis and cumulative distribution function (CDF) methods are used to explain the future uncertainties, instead of displaying the absolute results of each extreme indicator. The probability of future temperature extreme changes will be defined as being less than or greater than a given amount (Murphy et al. 2009; Programme 2009; Wang et al. 2014). Specifically, a cumulative probability of 10% is used to indicate the minimum acceptable level, namely the actual value that is very likely to be greater than or very unlikely to be less than the given amount. In contrast, the cumulative probability of 90% is used to indicate the maximum acceptable level, that is, the actual value is very likely to be less than or very unlikely to be greater than the current given value. In the same way, we regard the value with a cumulative probability of 50% as the most likely estimate of future projections. In this paper, we calculate three cumulative probability levels for each small spatial grid from the model ensemble to analyze their inter-annual changes.

### 2.4 Experimental design

The PRECIS ensemble simulations for the whole of China are carried out in a continuous run from 1950 to 2099 at a spatial resolution of 25 km, and then the time series is divided into four periods: the baseline period (1961–1990) for validation, the 2020s (2020–2040), 2050s (2041–2070) and 2080s (2071–2099) for projection. In the baseline period, owing to the different resolution between observations and model simulations, we have regridded the simulated results to the grid cells from observational datasets (0.5° horizontal

resolution) to facilitate the comparison. For the choice of study domain size, some climatic factors (i.e., summer and winter monsoon) that have primary effects on climate in China will be taken into account. The definitive domain extends from about 66.24°E–139.48°E and 10.07°N–54.34°N, which is over 38,000 25-km grid points in total (Fig. 1). In addition, the added value of regional climate modeling is the provision of fine-scale regional climate information, which is vital in the simulation of the frequency distribution of weather events and extremes (Torma et al. 2015). Thus, to validate the accuracy and credibility of PRECIS, several global climate models (Table 3) are compared with the projected results as well.

### 3 Results

#### 3.1 Model validation

To examine the performance of the five RCMs in representing China's current regional climatologically features of 16 extreme indices, the average annual simulations using PRECIS ensemble are compared with observations in spatial distributions from 1961 to 1990 (As shown Figs. 2, 3, 4, 5). Overall, the simulated distributions of all extreme indicators suggest that the PRECIS can reasonably reproduce the extreme temperature patterns in most regions of China, although there are some disagreements in some areas.

The spatial distributions in monthly warmest and coldest temperatures: warmest day, coldest day, warmest night and coldest night (hereinafter referred to as TXX, TXn,

**Fig. 1** Study domain. *Hatched lines* denote buffer zone area which is composed of eight grids along the longitude and latitude

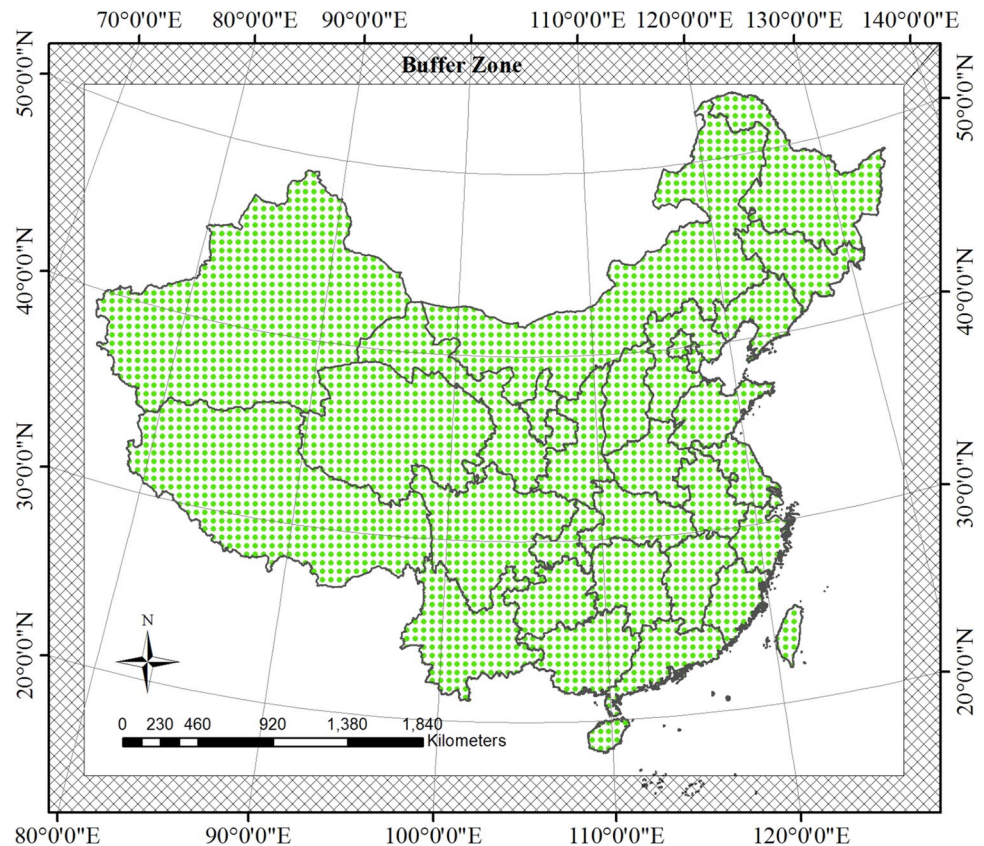


**Table 3** List of the GCMs used for comparison in this study

Model name	Time span	Resolution	Institute
BCM2.0	2001–2100	2.8° × 2.8°	Bjerknes Centre for Climate Research, Norway
MK3.5	2001–2200	1.875° × 1.875°	CSIRO Atmospheric Research, Australia
INMCM3.0	2001–2200	5° × 4°	Institute for Numerical Mathematics, Russia
MIROC 3.2	2001–2300	1.125° × 1.122°	CCSR/NIES/FRCGC
GISS model	2001–2100	4° × 3°	NASA
CCSM 3.0	2000–2099	1.4° × 1.4°	NCAR

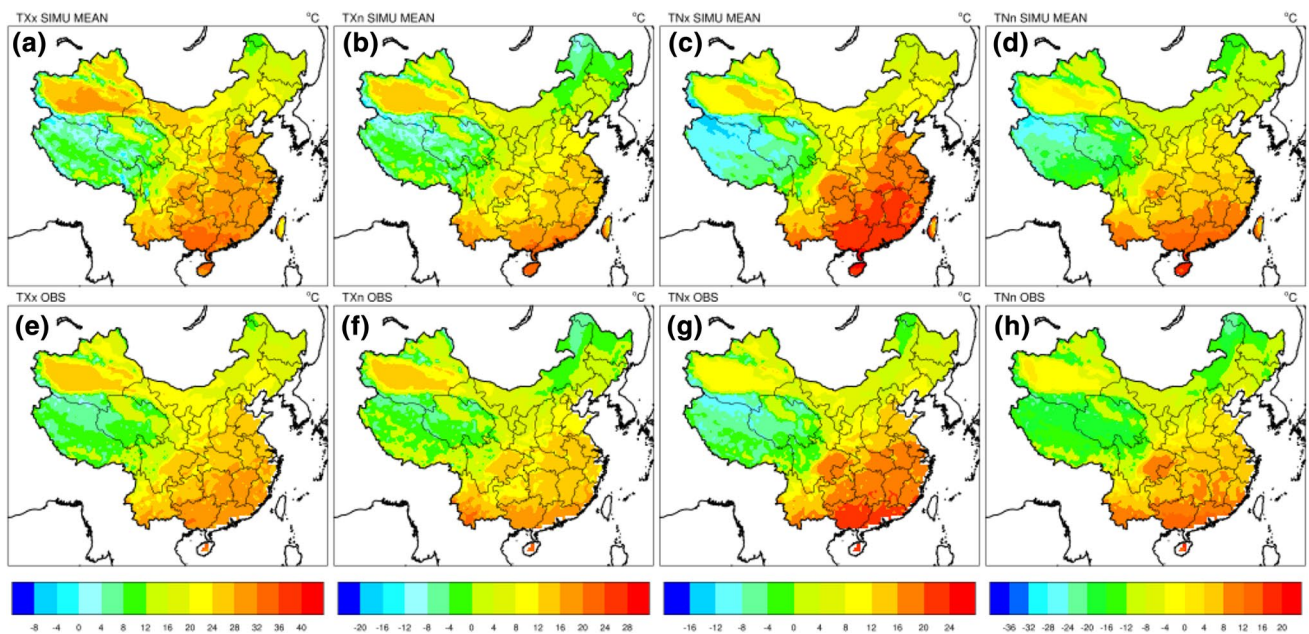


**Fig. 2** Spatial comparisons between simulations and observations over China for the TXx, TXn, TNx and TNn during the baseline period (1961–1990). The simulated values are the average of five RCMs ensemble (Q0, Q1, Q7, Q10 and Q13)

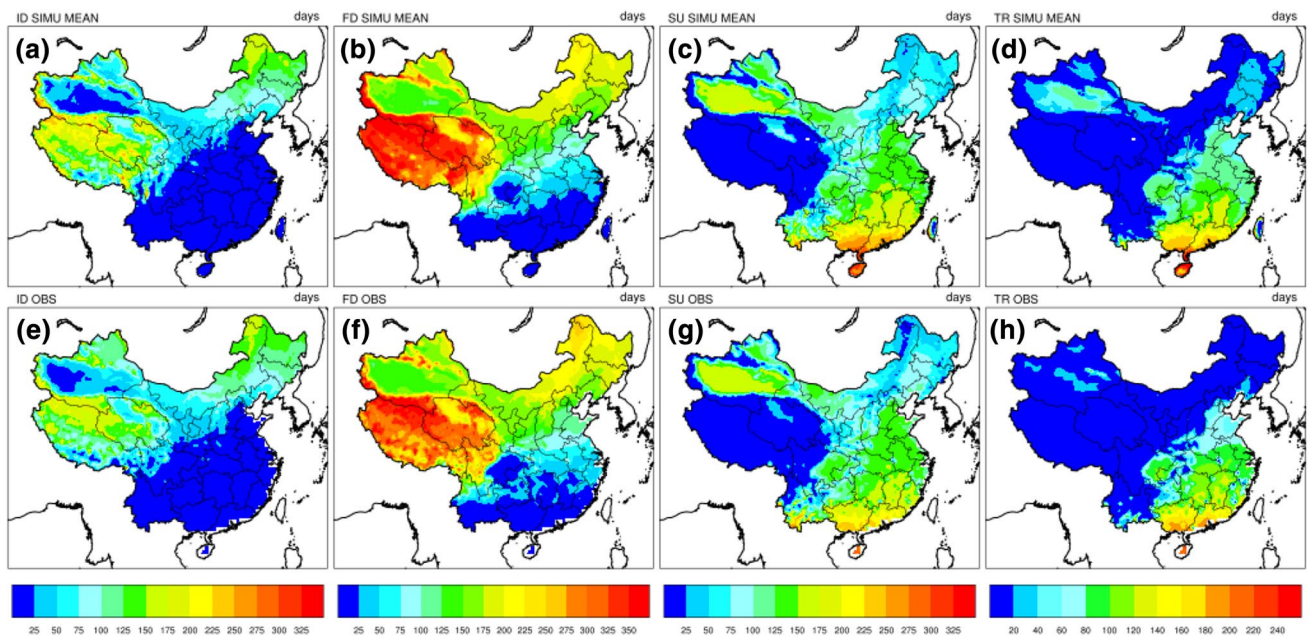


**Fig. 3** Spatial comparisons between simulations and observations over China for the ID, FD, SU and TR during the baseline period (1961–1990). The simulated values are the average of five RCMs ensemble (Q0, Q1, Q7, Q10 and Q13)

TNx and TNn), are shown as in Fig. 2. The results of the four simulated indices match well in spatial patterns with observations, with the warmest center appeared in the southeast and northwest and the coldest center located in the northeast and the Tibetan Plateau. For most regions of China, the biases between multi-model ensemble mean

and observations are maintained within in the range of  $[-2, 2]$  °C. However, prominent cold biases are conducted by RCMs in the west, especially in the marginal areas of the Tibetan Plateau and the south of the Himalayas (about 8 °C cold bias). While the monthly maximum temperature indices (TXx and TXn) are overestimated (about 6 °C) in the

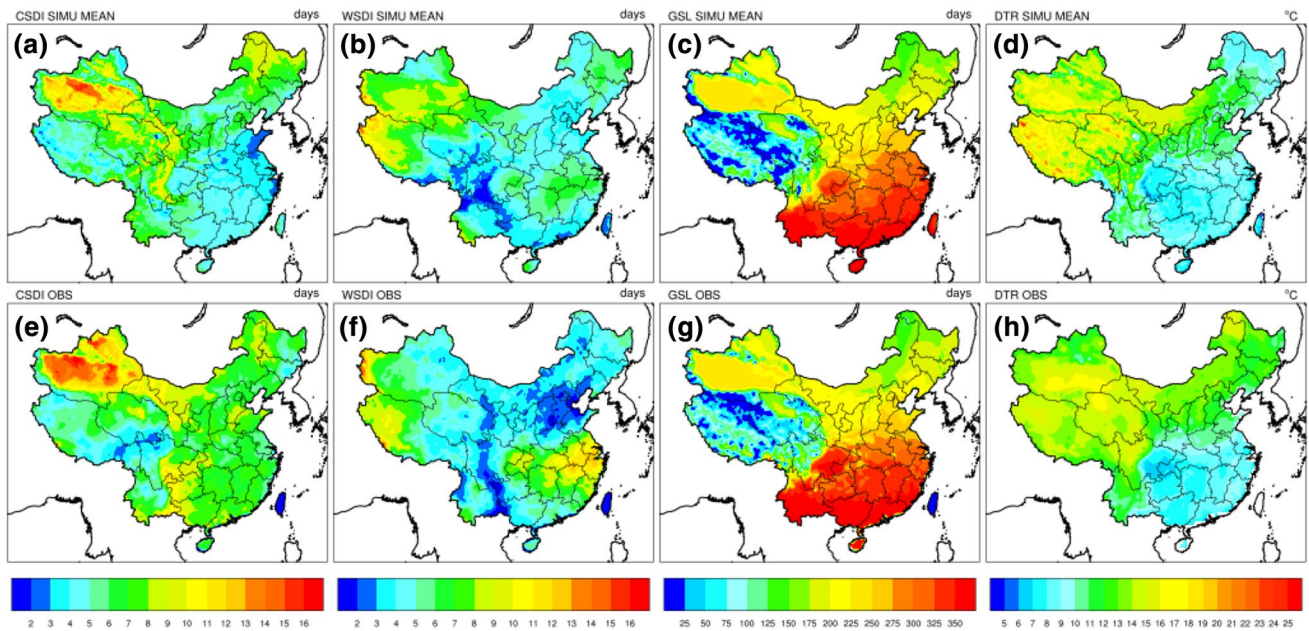


**Fig. 4** Spatial comparisons between simulations and observations over China for the CSDI, WSDI, GSL and DTR during the baseline period (1961–1990). The simulated values are the average of five RCMs ensemble (Q0, Q1, Q7, Q10 and Q13)

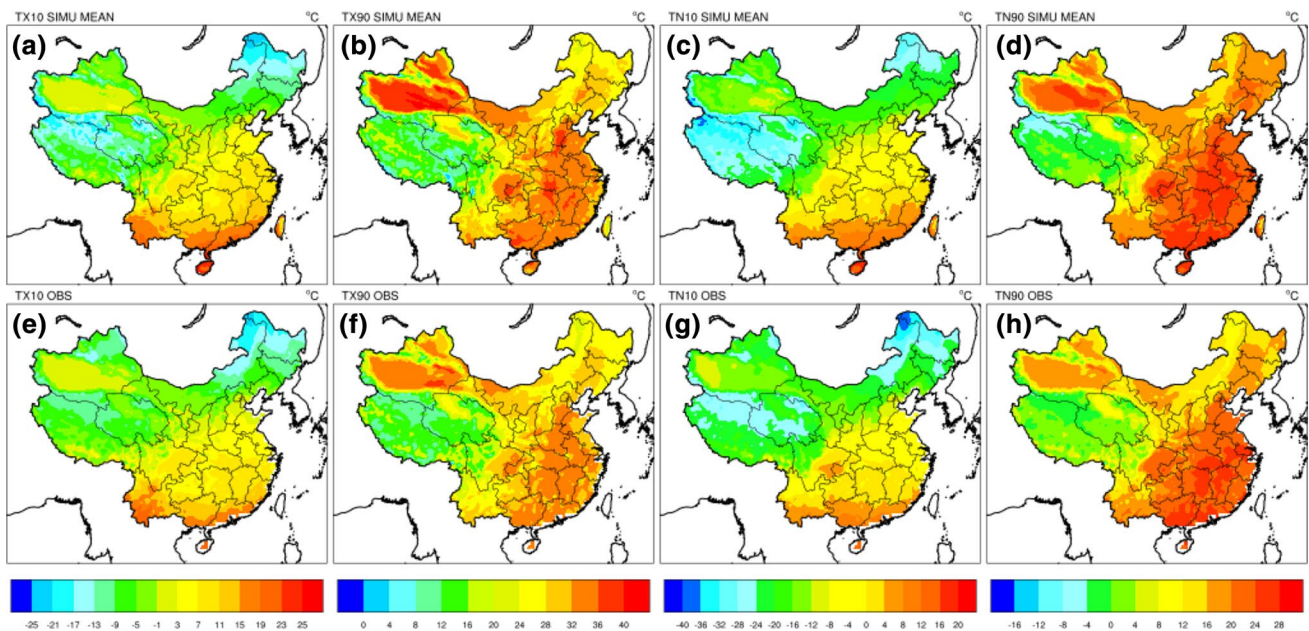


**Fig. 5** Spatial comparisons between simulations with observations over China for the TX10, TX90, TN10 and TN90 during the baseline period (1961–1990). The simulated values are average of five RCMs ensemble (Q0, Q1, Q7, Q10 and Q13)

northwest of Xinjiang and the monthly minimum temperature indices (TNx and TNn) exhibit warm biases in parts of the northeast and Sichuan region.

Compared with the observations, RCMs can well simulate the spatial patterns of four fixed threshold-based indices, such as ID, FD, SU and TR (Fig. 3).

Specifically, the simulated summer days (SU) are closer to the observed values than the other three indicators. In the southeast, the ice days (ID), frost days (FD) and tropical nights (TR) are slightly underestimated, but overestimated in most western regions, particularly for TR in the Tibetan Plateau.

For the four spell duration indices, the results show that PRECIS has the ability to capture the distributions of baseline period in most parts of China (Fig. 4). However, as discussed in previous indices, there are some more or less biases in some areas. For example, the simulated cold spell duration index (CSDI) is a bit shorter than the observed value. For the warm spell duration index (WSDI), the satisfactory results from PRECIS are obtained with a deviation of 1–2 days in the central and southwest, but the simulations are underestimated on the southeast regions (~[3, 4] days). On the maps of the glowing season length (GSL), the southern observed GSL is shorter than simulations, except for the south of Qinghai. There is a relatively narrow daily temperature range (DTR) for simulations in the north and the Tibetan Plateau.

When calculating four relative indices, such as cold days (TX10p), warm days (TX90p), cold nights (TN10p) and warm nights (TN90p), it is desirable first to determine the reference time. Since the baseline period is the same as the reference time, instead directly of verifying these indices, we use other alternative percentile indices (i.e., TX10, TX90, TN10 and TN90) to test simulated ability. In the comparison for TX10 and TX90, the simulated results are somewhat larger than the actual ones, especially in most parts of Xinjiang. This may be some of the underestimation of the TX10, but the valuation in northern China is too high.

In addition, the PLCC and the NSE of each index are calculated to validate the performance of PRECIS (Fig. 6). Overall, the PLCC values of most indices remain at around 0.9, indicating the simulations and observations are highly correlated. Moreover, all indices have a high NSE value except for CSDI, WSDI and DTR. However, the overall averaged rating (AR) of 16 indices is 0.81, suggesting the simulated results are good according to the defined rating table.

In general, PRECIS has the ability to reproduce 16 temperature extreme indices in spatial distribution during the baseline period, and shows better performance in eastern China. There are more biases in the west,

especially in the Tibetan Plateau. Some of the reasons that are inconsistent with observations may be partly attributed to the lack of observation itself and the uncertainties of LBCs in high topography or isolated areas besides from model biases (Yu et al. 2014).

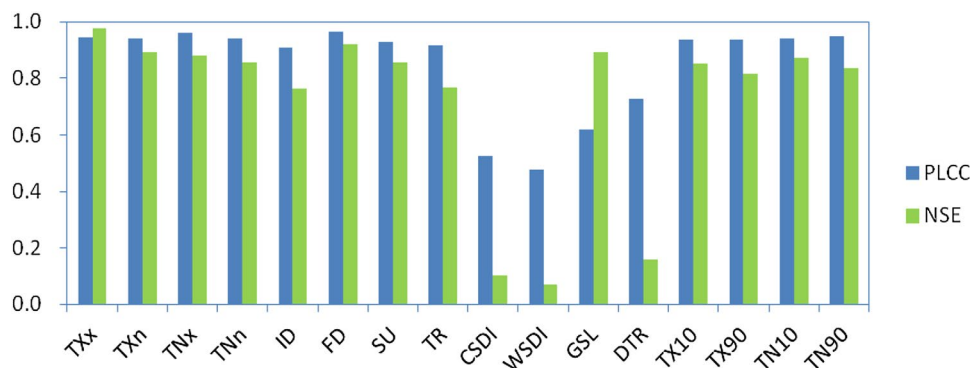
### 3.2 Changes for extreme indices

Here we divided the simulated results into three continuous 30-year periods throughout the twenty-first century: 2011–2040 (or 2020s), 2041–2070 (or 2050s), and 2071–2099 (or 2080s). For each extreme index, the projected spatial and temporal changes for three future periods are discussed in the following sections. In addition, the PRECIS simulations will be compared to other GCMs (i.e., BCM2.0, MK3.5) to investigate whether PRECIS predictions are consistent with these GCMs and what are the added values of PRECIS simulations at regional and local scales in the context of China.

#### 3.2.1 Comparison with other GCMs

As shown in Figs. 7 and 8, the results of RCMs ensemble are essentially in agreement with the GCMs in the spatial distribution and variability over time. Both RCMs and GCMs show the low temperature center in Tibet and northeast regions and the high temperature belt from northwest to southeast. However, it is clear that the simulations from RCMs ensemble can provide more detailed information in spatial distribution, which is ignored or omitted in GCMs owing to its low resolution. In terms of time, from 2011 to 2099, both have almost a similar trend, the daily maximum temperature is expected to increase from 15 to 19 °C and the daily minimum temperature would rise from 5 to 10 °C. Nevertheless, the simulated temperature is slightly lower than GCMs before 2040, but then it gradually begins to catch up and eventually get ahead.

**Fig. 6** PLCC and NES values between simulations and observations



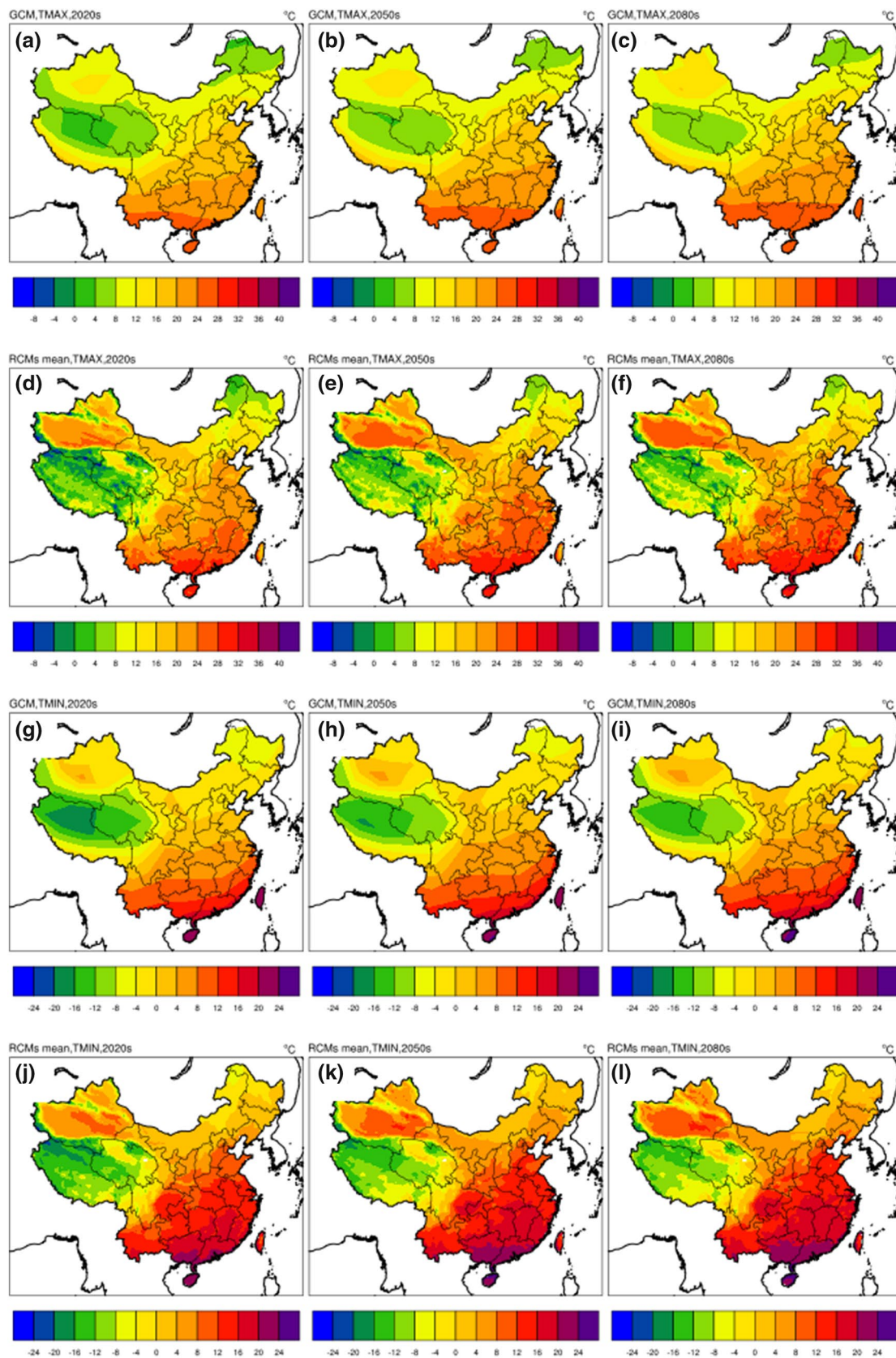
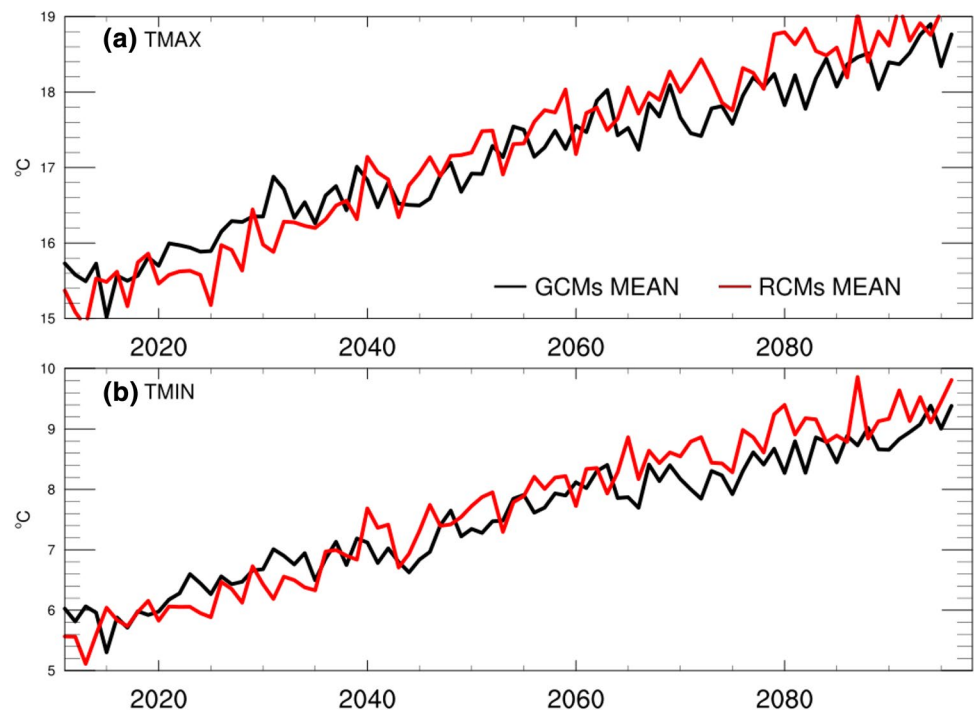


**Fig. 7** Spatial comparisons between GCMs and RCMs in the daily maximum and minimum temperature. **a–c** and **g–i** represent the average of GCMs. **d–f** and **j–l** represent the average of RCMs ensemble. Columns from left to right are shown as 2020s, 2050s and 2080s, respectively

**Fig. 8** Annual trends between GCMs and RCMs in the daily maximum and minimum temperature



### 3.2.2 Future spatial distribution changes for extreme indices

**3.2.2.1 Monthly extremal indices** Compared with the baseline period, four monthly maximum and minimum temperature indices show a significant growth trend in the next three periods. At the beginning of this century, the most likely temperature rise for the warmest day (TXx) and warmest night (TNx) over the whole of China would be [1, 2] °C. The increase of the coldest day (TXn) is relative small (only 0.5 °C) in central Yunnan. The TNx and TNn have distinctive regional patterns, which display higher in the north than in the south along latitude, especially for TNn in the northwest (about [2.5, 3] °C). In 2050s, the spatial distribution characteristics are generally similar to that in 2020s, but the magnitude of increase is greater. For instance, during this period, the TXx and TXn grow at about [3, 4] °C and TNx shows the largest increase in south-central China. By the late 21st century, the four indices increase will remain at around [2, 5] °C but the increments gradually decrease relative to the first two periods, particularly in the south. However, the TNn shows a great potential increase in north in this period ([5.5, 6] °C) (Fig. 9).

**3.2.2.2 Fixed threshold-based indices** Another notable warming in China is reflected in four fixed threshold-based indices. From the early years of the twenty first century, the annual icing days (ID) and frost days (FD) will gradually decrease, especially in marginal areas of southwest, while there is an obvious growing trend for summer days (SU)

and tropical nights (TR) in some regions of Yunnan. The annual durations of ID and FD will be further shortened in the middle and late periods. For example, the number of these measures will be reduced by about 40 days relative to the baseline period in southwest. On the contrary, SU and TR in the same region do not change much and the increase in these indices is mainly concentrated in the northwest and Yunnan (Fig. 10).

**3.2.2.3 Spell duration indices** In addition to several regions, the warm spell duration index (WSDI) and cold spell duration index (CSDI) exhibit a rising trend in the future but slowing down (about 1 day per year). In the 2050s, CSDI would be gradual upward in the northeast, northwest and parts of Yunnan, while remarkable downward across some areas in Shanxi and Shaanxi. The daily temperature range (DTR) will show a decreasing trend in the north, but little changes in the south. Compared with the 2020s, the northern DTR will keep a trend of decline in the next two periods (about 1 °C decrease). Three apparent zones are separated from the latitude for the growing season length (GSL), namely, the fastest growing in the central, the next in the north, and the least in the south. It is worth mentioning that the growing season may grow by about 50 days in the mid-west regions of China by the end of this century (Fig. 11).

**3.2.2.4 Percentile-based indices** Compared to the baseline period, four percentile-based indices, such as cold days (TX10p), warm days (TX90p), cold nights (TN10p) and

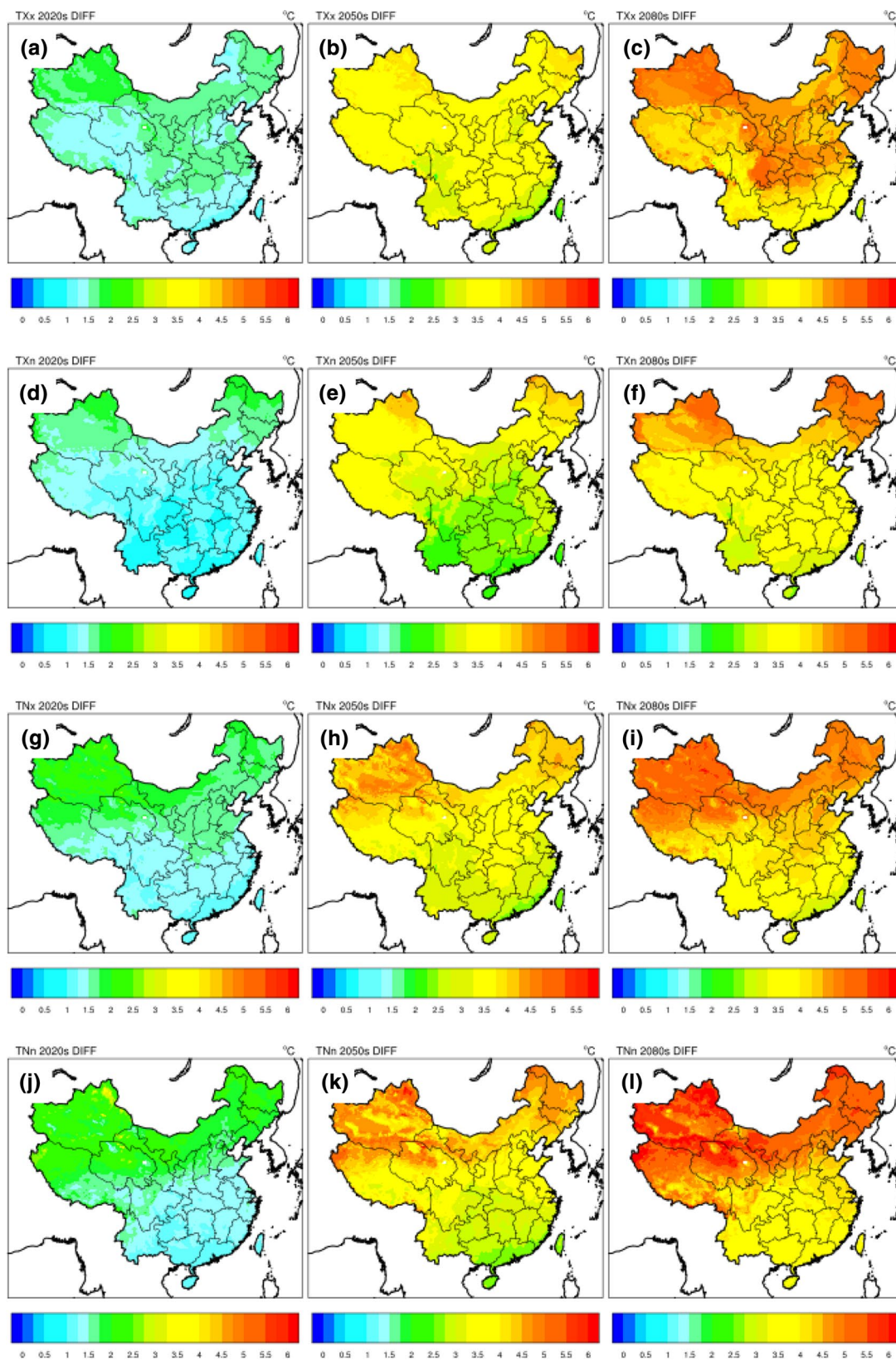


**Fig. 9** Changes in spatial distribution for the TXx, TXn, TNx and TNn. Columns from left to right are shown as 2020s, 2050s and 2080s, respectively

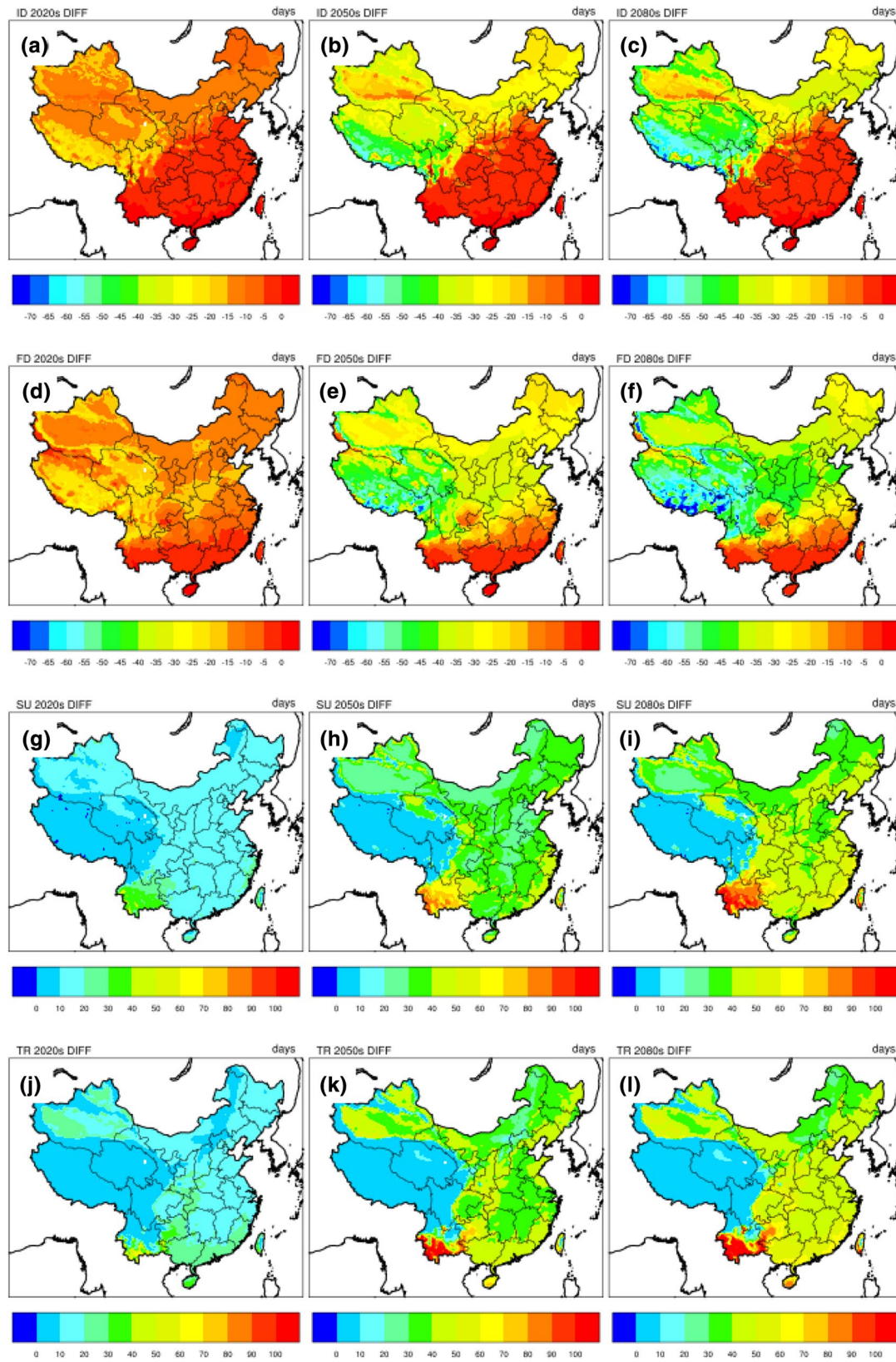


**Fig. 10** Changes in spatial distribution for the ID, FD, SU and TR. Columns from left to right are shown as 2020s, 2050s and 2080s, respectively

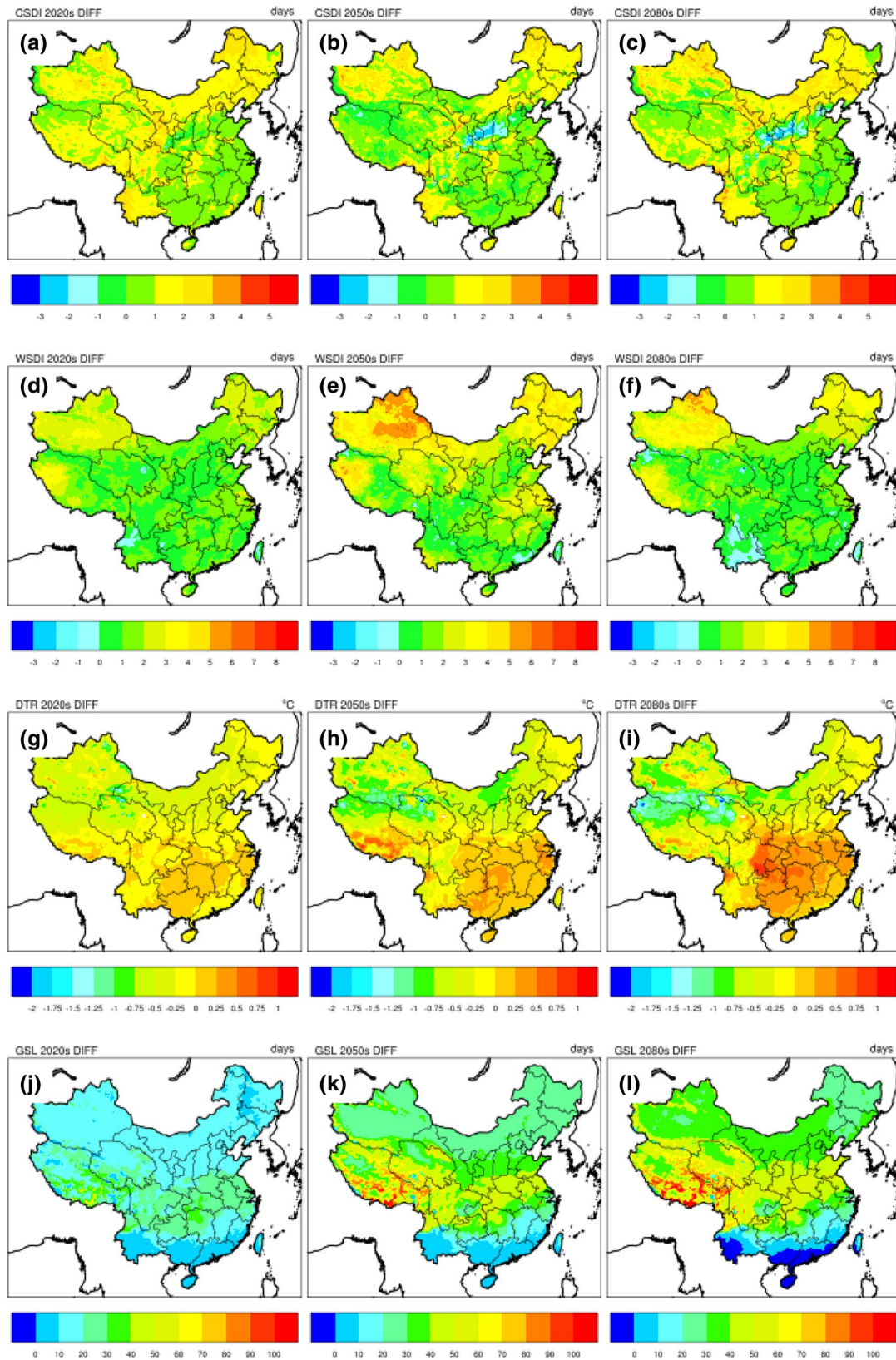
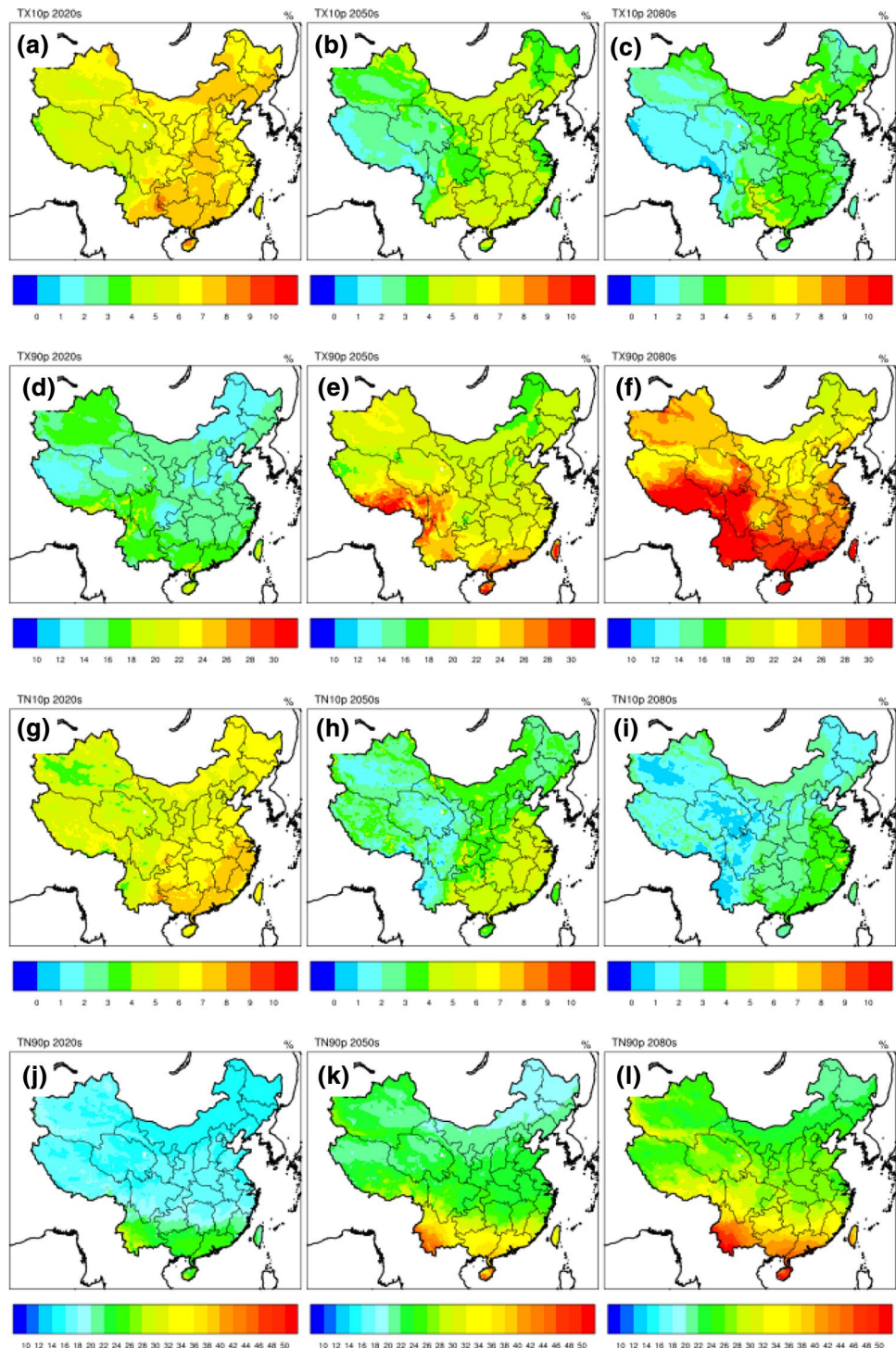


**Fig. 11** Changes in spatial distribution for the WSDI, CSDI, DTR and GSL. Columns from left to right are shown as 2020s, 2050s and 2080s, respectively

warm nights (TN90p), will appear to increase for the next three periods. These indices will be divided into two categories according to their trends from 2020s: upward for TX10p and TN10p and downward for TX90p and TN90p. TX10p in western China will be falling more than the east from 2050s and probably remain pretty much the same with the baseline period by the end of the century. It is noted that the overall tendency of TN10p is in accordance with TX10p, with 7,

5 and 4% changes in southeast for the next three periods, respectively. In contrast, warm days and warm nights indicate a gradually increase. For example, the TX90p will grow by 15% in the 2020s, 25% in the 2050s and 30% in the 2080s over the southwest. Moreover, the growth of warm nights will be more pronounced in the south of Yunnan, Guangdong and Guangxi, or even up to 40% (Fig. 12).

**Fig. 12** Changes in spatial distribution for TX10p, TX90p, TN10p and TN90p. Columns from left to right are shown as 2020s, 2050s and 2080s, respectively



In summary, all extreme indices will have less change in the south than most northern areas, where it may experience milder winter and hotter summers in the future. In the context of global warming, both daily maximum and minimum temperature begin to rise to a certain extent with time. The changes of some extreme indicators, such as ID, FD, SU, TR and GSL, are proof of warming from another way. Some indices have obvious spatial distribution characteristics. For example, ID, FD and GSL exhibit a larger increasing trend in the west than in other regions, while SU and TR display decreasing trend, especially in Yunnan. Likewise, the results from four percentile-based indices demonstrate that the projected changes in extreme temperature in the north are apparently higher than the changes in the west. Nevertheless, the changes in the rest indices (i.e., CSDI, WSDI and DTR) are barely perceptible as just mentioned ones in space.

### 3.2.3 Inter-annual changes for extreme indices

During the first 30-year period, the predictions for TX<sub>x</sub>, TX<sub>n</sub>, TN<sub>x</sub> and TN<sub>n</sub> show that the most likely monthly extreme temperature will grow at about 0.05 °C per year throughout China. The changes in ID and FD are opposite to those of SU and TR. Compared with the baseline period, ID and FD have decreased about 10 days in 2011, and the number will drop even further with the rate of around 0.3 day a year. While SU and TR appear an upward tendency, from 8 days in 2011 to 18 days in 2040. Although the CSDI shows a slight decrease while WSDI presents an increase, the trends for two spell duration indices are not obvious in the early years of twenty-first century. As the daily maximum and minimum temperatures rise, the DTR is almost unchanged relative to the baseline period. However, the growing season will expand [5, 10] days. The four relative indices will increase obviously in 2011, by [5, 10] % for the cold indexes (i.e., TX<sub>10p</sub> and TN<sub>10p</sub>) and [10, 17] % for the warm indexes (i.e., TX<sub>90p</sub> and TN<sub>90p</sub>). From 2011, the TX<sub>10p</sub> and TN<sub>10p</sub> will show a decreasing tendency while TX<sub>90p</sub> and TN<sub>90p</sub> will gradually increase with time, especially for TN<sub>90p</sub> at the annual rate of 0.216% increase (Fig. 13).

As shown in Fig. 14, the trends for all extreme indices in the middle of this century are in agreement with those in the former period. For example, the four monthly extreme indices (i.e., TX<sub>x</sub>, TX<sub>n</sub>, TN<sub>x</sub> and TN<sub>n</sub>) will increase [2, 4] °C compared to the baseline, while ice days and frost days will be reduced by 22 and 32 days, respectively. The WSDI and GSL may continue to rise about 3 and 15 days. The rate of decline for TX<sub>10p</sub> and TN<sub>10p</sub> begin to slow, while the corresponding increase rate of TX<sub>90p</sub> and TN<sub>90p</sub> will be faster in this period.

In the 2080s, the trends for most indices show a clear sign of slowness (Fig. 15). Compared with the baseline period, the changes of monthly extreme indices seem to be maintained within about 4 °C; moreover, ice days and frost days will be kept in 25 and 35 days or so. Apart from two warm relative indices, other indicators have little change in the end of this century. However, it is important to note that the distances between 90 and 10% probability levels (gray band between two green lines) are larger for most indices in this period than the first two periods, implying that there are more disagreements among models for long-term simulations.

Overall, the 16 indices of extreme temperature have basically the same tendency in the next three periods, though with different rates of change, and in the near-term the change rate is highest, a bit lower in mid-term and lowest in the end of this century. The changes of these indices support the conclusion that the temperature is rising over the whole of China under the background of global warming (Table 4).

## 4 Conclusions

In this study, potential changes in extreme temperatures (including 16 indices) over China in response to global warming throughout the twenty-first century are investigated through the PRECIS regional climate modeling system. In order to reflect the uncertainties caused by its driving boundary conditions, the PRECIS model is driven by a perturbed-physics ensemble from the UK Met Office HadCM3 model. The spatial resolution of the PRECIS ensemble simulations is 25 km with the purpose of reflecting the spatial variations of temperature extremes in the context of China.

During the baseline period (1961–1990), the simulated results are compared with the observational gridded data sets, provided by National Meteorological Information Center (NMIC), China. Overall, the results indicate that the PRECIS is able to reasonably reproduce the spatial patterns of current extreme temperatures over most regions of China, especially in the east. For example, simulated four monthly extremal indices (TX<sub>x</sub>, TX<sub>n</sub>, TN<sub>x</sub> and TN<sub>n</sub>) are agreement well with observations in the spatial patterns, with average biases keeping in the range of [-2, 2] °C. The simulated results for summer days and cold spell duration index are satisfactory as well. However, some extreme indices appear a relatively large difference in the western areas. For example, TX<sub>x</sub>, TX<sub>n</sub>, TN<sub>x</sub> and TN<sub>n</sub> present obvious cold biases in the mountainous areas of the Tibetan Plateau and southern of the Himalayas. Nevertheless, the projections of three absolute indices (i.e., ID, FD and TR) are apparent overesti

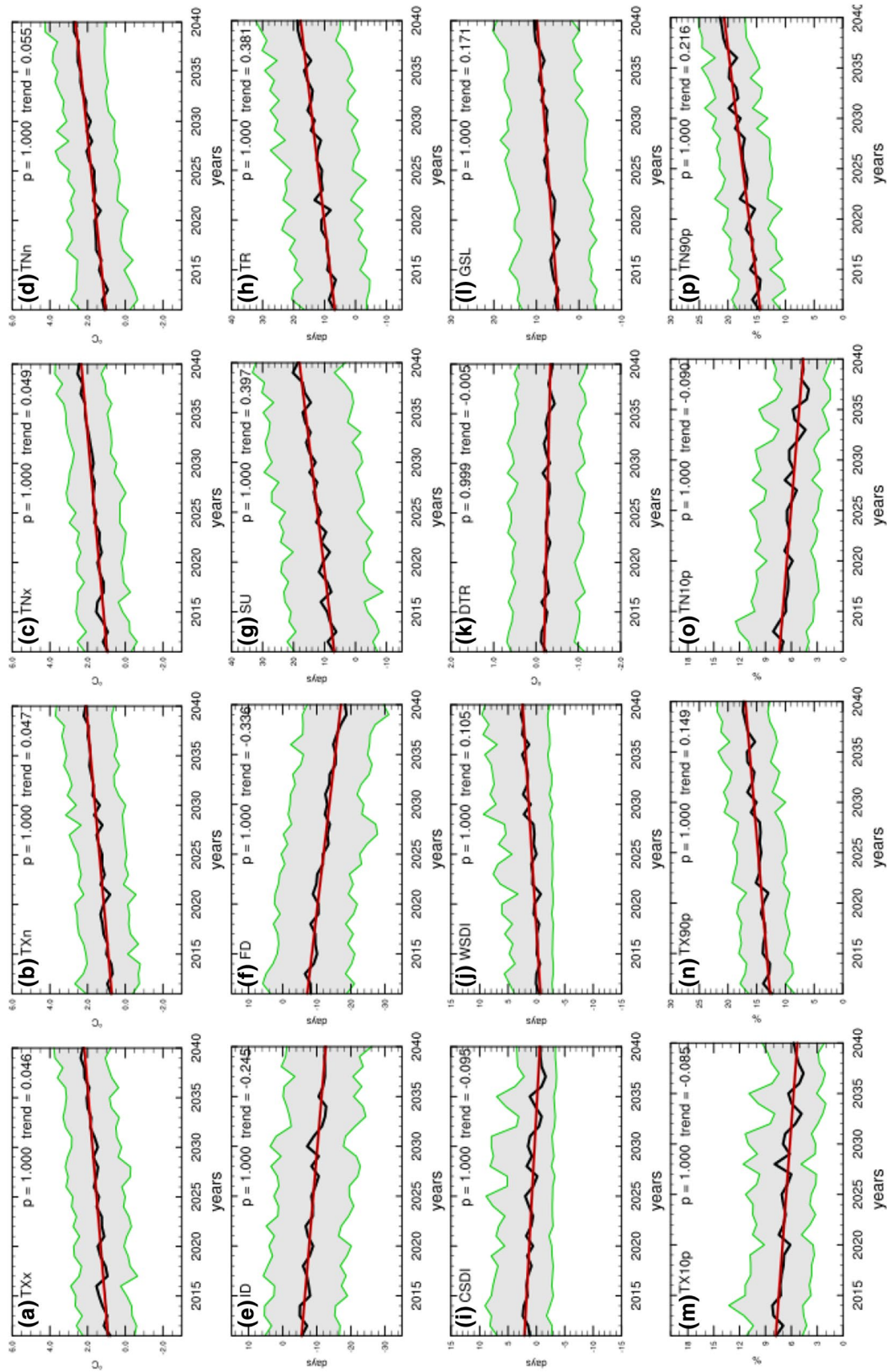


**Fig. 13** Trends for all extreme indices in 2020s. The black line represents a 50% probability level and the top and bottom green lines are shown as a probability level of 90% and 10%, respectively

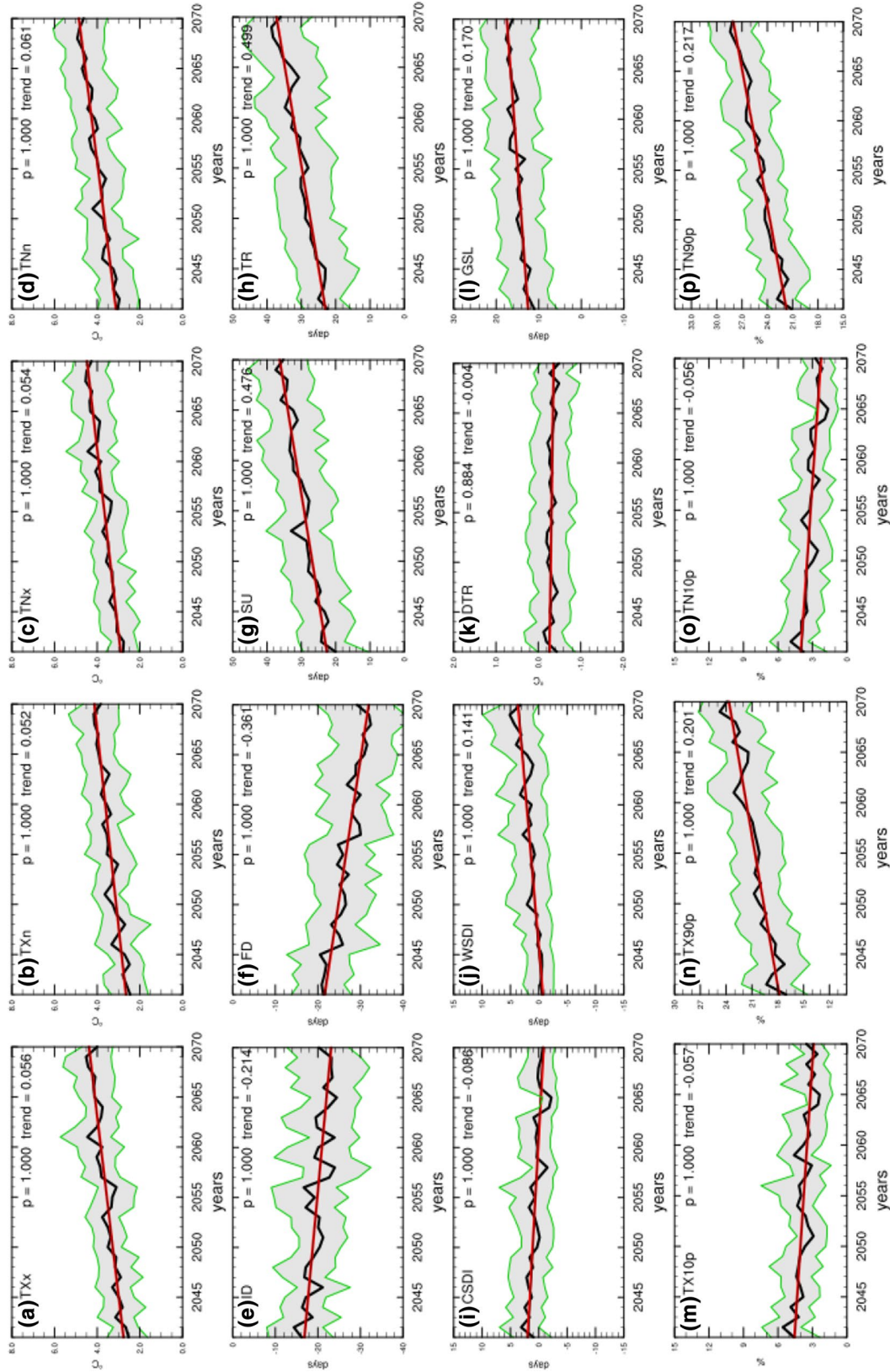


**Fig. 14** Trends for all extreme indices in 2050s. The black line represents a 50% probability level and the top and bottom green lines are shown as a probability level of 90 and 10%, respectively

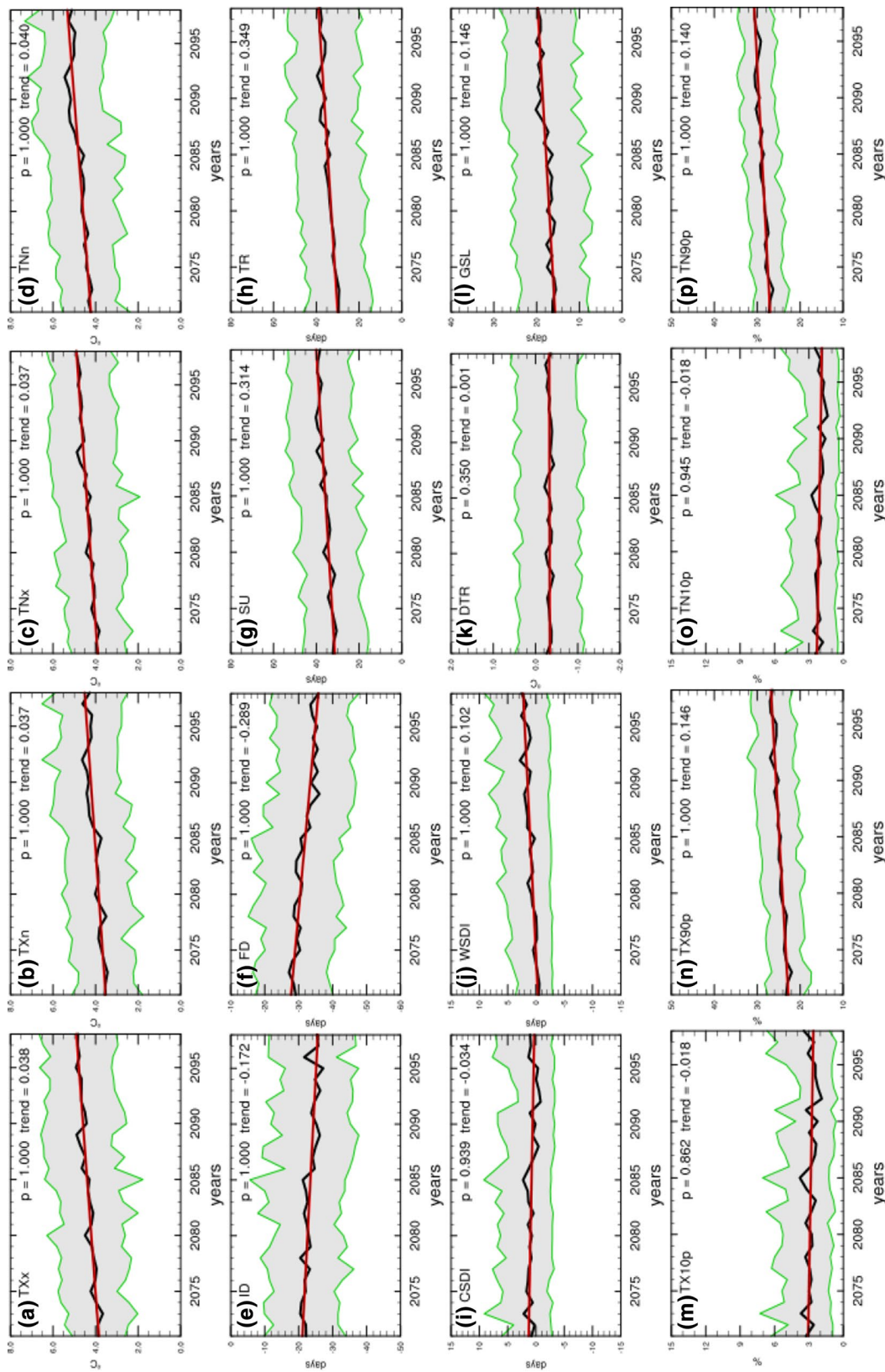


**Fig. 15** Trends for all extreme indices in 2080s. The black line represents the 50% probability level and the top and bottom green lines are shown as a probability level of 90 and 10%, respectively

**Table 4** Projected changes for 16 extreme indices over the whole of China relative to the baseline period at 10, 50 and 90% probability levels

	Monthly extreme indices				Fixed threshold-based indices				Spell duration indices				Percentile-based indices			
	TXx	TXn	TNx	TNn	ID	FD	SU	TR	CSDI	WSDI	DTR	GSL	TX10p	TX90p	TN10p	TN90p
	2020s															
10%	-1.722	-2.311	-1.241	-1.548	-19.884	-23.108	-2.015	-0.073	-2.924	-2.657	-1.058	-1.58	2.873	13.308	3.440	10.599
50%	1.544	1.395	1.652	1.836	-9.080	-12.144	12.486	12.214	0.754	0.870	-0.264	7.353	5.998	17.521	6.554	14.833
90%	4.808	4.962	4.531	5.036	1.828	-0.785	25.448	23.877	6.276	6.508	0.553	16.143	9.607	21.563	10.199	19.082
2050s																
10%	2.684	2.517	2.852	2.991	-26.741	-33.844	21.467	21.494	-2.145	-1.468	-0.762	9.326	1.670	22.340	2.203	17.834
50%	3.577	3.394	3.691	3.991	-19.970	-26.769	29.451	30.128	0.551	1.472	-0.312	15.014	3.132	24.894	3.731	20.755
90%	4.445	4.249	4.479	4.920	-13.020	-19.268	37.041	37.954	3.729	4.961	0.144	20.579	4.753	27.359	5.403	23.588
2080s																
10%	2.818	2.558	2.905	3.202	-34.811	-44.724	20.474	18.495	-2.916	-2.523	-1.064	8.957	0.507	24.923	0.959	20.231
50%	4.478	4.106	4.491	4.864	-24.198	-33.253	35.588	34.608	0.713	1.025	-0.325	17.367	2.055	28.914	2.796	24.842
90%	6.116	5.636	5.913	6.404	-12.477	-21.470	49.587	49.251	6.056	6.142	0.447	25.701	4.338	32.778	5.390	29.486

mated on the same regions. Some reasons for these disagreements with observations may be partly attributed to the lack of observation itself and the uncertainties of LBCs in high topography or isolated areas besides from model biases (Yu et al. 2014).

Future spatio-temporal changes of temperature extreme indices as simulated by PRECIS for three successive 30-year periods in the twenty-first century are presented in this paper. The results indicate the following aspects:

1. The simulative results from the PRECIS for daily maximum and minimum temperature are in good agreement with the outcomes from global climate models in both spatial and temporal patterns. Furthermore, it is pronounced that the PRECIS demonstrates a distinct superiority in providing more small-scale detail features especially in the regions of immense complexity.
2. In general, there is a consistent spatial pattern for all extreme indices: large changes are projected in the north while small changes are projected in the south compared with the baseline period. The results show that the future ice days and frost days will decrease from north to south, while summer days, tropical nights and growing season length will increase to different degrees. Meanwhile, the findings also suggest that there would be a larger increasing trend in temperature extremes in the north and west. This is generally consistent with several previous studies (Sun et al. 2016; Zhang et al. 2011; Zhou et al. 2014), however, for some indices (i.e., TNn) the increase amplitude (i.e., [5.5, 6] °C) is slightly lower than these studies (i.e., exceeding 7 °C) in the north by the end of the twenty-first century.
3. The temporal patterns for all indices vary differently over future periods. Specifically, the warm indices, such as SU, TR, WSDI, TX90p, TN90p and GSL are likely to increase while some cold indices, such as ID, FD, CSDI, TX10P and TN10p, are likely to decrease with time relative to the baseline period. These changes are strongly consistent with other similar studies in other regions regarding their response to global warming (Alexander et al. 2006; Choi et al. 2009; Zhang et al. 2017a), however, this study can provide more detail information on future changes in temperature extremes in China due to its high-resolution and multi-model prediction. Although the amplitudes of variation are different among the indices in future, the rates of changes tend to gradually decrease. For example, the TXx increases by 1.544 °C in 2020s, 3.577 °C in 2050s and 4.478 °C in 2080s at 50% probability level. In addition, the projected ranges of changes for all indices would become larger with time, suggesting more uncertainties would be involved in long-term climate projections.

In summary, the results from this paper in providing more detailed information at regional and local scales in the context of China could be the biggest values compared with other studies. The modelling experiment is verified to an acceptable level, and the experimental output can provide resource or economic planners and managers some valuable suggestions for the assessment of impacts and implementation of adaptation measures in China. In addition, we also discussed the limitations of the data and provided information on how to use the maps and output, for example, some indices (i.e., CSDI, WSDI and DTR) exist greater experimental errors in the certain regions of China, and thus the decision to use these data requires careful consideration. Moreover, the multi-model ensemble with high resolution is an important pathway for capturing and reducing uncertainties in climate simulations and projections. The methods and routes employed here could extend to other extreme indices in different regions.

**Acknowledgements** This research was supported by the National Key Research and Development Plan (2016YFA0601502, 2016YFC0502800 and 2016YFE0102400), Fundamental Research Funds for the Central Universities (2017MS049), Natural Sciences Foundation (51190095, 51225904), the Program for Innovative Research Team in University (IRT1127), the 111 Project (B14008), the National Basic Research Program (2013CB430401), Ontario Ministry of the Environment and Climate Change, and the Natural Science and Engineering Research Council of Canada.

## References

- Ahmed SM (2014) Assessment of irrigation system sustainability using the Theil–Sen estimator of slope of time series. *Sustainability Sci* 9:293–302
- Alexander LV, Zhang X, Peterson TC, Caesar J, Gleason B, Klein Tank AMG, Haylock M, Collins D, Trewin B, Rahimzadeh F (2006) Global observed changes in daily climate extremes of temperature and precipitation. *J Geophys Res Atmos* 111:1042–1063
- Araghi A, Mousavi-Baygi M, Adamowski J (2016) Detection of trends in days with extreme temperatures in Iran from 1961 to 2010. *Theor Appl Climatol* 125:213–225
- Beharry SL, Clarke RM, Kumarsingh K (2015) Variations in extreme temperature and precipitation for a Caribbean island: Trinidad. *Theor Appl Climatol* 122:783–797
- Beniston M, Stephenson DB, Christensen OB, C.A.T. Ferro, Frei C, Goyette S, Halsnaes K, Holt T, Jylhä K, Koffi B (2007) Future extreme events in European climate: an exploration of regional climate model projections. *Clim Change* 81:71–95
- Bian T, Ren G, Zhang B, Zhang L, Yue Y (2015) Urbanization effect on long-term trends of extreme temperature indices at Shijiazhuang station, North China. *Theor Appl Climatol* 119:407–418
- Buontempo C, Mathison C, Jones R, Williams K, Wang C, Mcsweeney C (2014) An ensemble climate projection for Africa. *Clim Dyn* 44:1–22
- Busuoioc A, Chen D, Hellström C (2001) Performance of statistical downscaling models in GCM validation and regional climate change estimates: application for Swedish precipitation. *Int J Climatol* 21:557–578
- Cardil A, Molina DM, Kobziar LN (2014) Extreme temperature days and their potential impacts on southern. *Eur Nat Hazards Earth Syst Sci* 14:3005–3014
- Cheng L, Phillips TJ, Aghakouchak A (2015) Non-stationary return levels of CMIP5 multi-model temperature extremes. *Clim Dyn* 44:2947–2963
- Choi G, Collins D, Ren G, Trewin B, Baldi M, Fukuda Y, Afzaal M, Pianmana T, Gomboluudev P, Huong PTT (2009) Changes in means and extreme events of temperature and precipitation in the Asia-Pacific Network region, 1955–2007. *Int J Climatol* 29:1906–1925
- Collins M, Booth BBB, Harris GR, Murphy JM, Sexton DMH, Webb MJ (2006) Towards quantifying uncertainty in transient climate change. *Clim Dyn* 27:127–147
- Déqué M (2007) Frequency of precipitation and temperature extremes over France in an anthropogenic scenario: model results and statistical correction according to observed values. *Global Planetary Change* 57:16–26
- Diaz JH (2007) The influence of global warming on natural disasters and their public health outcomes. *Am J Disaster Med* 2:33–42
- Etterson JR, Shaw RG (2001) Constraint to adaptive evolution in response to global warming. *Science* 294:151–154
- Filahi S, Tanarhte M, Mouhir L, Morhit ME, Trambly Y (2016) Trends in indices of daily temperature and precipitations extremes in Morocco. *Theor Appl Climatol* 124:959–972
- Fioravanti G, Piervitali E, Desiato F (2016) Recent changes of temperature extremes over Italy: an index-based analysis. *Theor Appl Climatol* 123:473–486
- Fonseca D, Carvalho MJ, Marta-Almeida M, Melo-Gonçalves P, Rocha A (2015) Recent trends of extreme temperature indices for the Iberian Peninsula. *Phys Chem Earth Parts A/b/c* 94:66–76
- Grotjahn R, Black R, Leung R, Wehner MF, Barlow M, Bosilovich M, Gershunov A, Gutowski WJ, Gyakum JR, Katz RW (2016) North American extreme temperature events and related large scale meteorological patterns: a review of statistical methods, dynamics, modeling, and trends. *Clim Dyn* 46:1151–1184
- Guan Y, Zheng F, Zhang X, Wang B (2015) Trends and variability of daily precipitation and extremes during 1960–2012 in the Yangtze River Basin, China. *Glob Planet Change* 124:79–94
- Hamed KH, Rao AR (1998) A modified Mann-Kendall trend test for autocorrelated data. *J Hydrol* 204:182–196
- Hartmann CLADL, Brönnimann S, Dentener FJ, Dlugokencky EJ, Easterling DR, Kaplan A, Soden BJ (2014) IPCC (2013), Climate Change 2013, in The Physical Science Basis, Working Group I Contribution to the Fifth Assessment Report of the Intergovernmental Panel on Climate Change, WMO/UNEP, Cambridge
- Iqbal MA, Penas A, Canoortiz A, Kersebaum KC, Herrero L, Del Río S (2016) Analysis of recent changes in maximum and minimum temperatures in Pakistan. *Atmos Res* 168:234–249
- Jiang C, Mu X, Wang F, Zhao G (2015) Analysis of extreme temperature events in the Qinling Mountains and surrounding area during 1960–2012. *Quatern Int* 392:129–138
- Karim MR, Rahman MA (2015) Drought risk management for increased cereal production in Asian Least Developed Countries. *Weather Clim Extremes* 3:24–35
- Khan U, Valeo C (2016) Short-term peak flow rate prediction and flood risk assessment using fuzzy linear regression. *J Environ Inform* 28:71–89
- Kim YH, Min SK, Zhang X, Zwiers F, Alexander LV, Donat MG, Tung YS (2015) Attribution of extreme temperature changes during 1951–2010. *Clim Dyn* 46:1769–1782
- Kitoh A, Endo H (2016) Changes in precipitation extremes projected by a 20-km mesh global atmospheric model. *Weather Clim Extremes* 11:41–52

- Liang K, Peng B, Li J, Liu C (2014) Variability of temperature extremes in the Yellow River basin during 1961–2011. *Quatern Int* 336:52–64
- Lü J, Ju J, Ren J, Gan W (2012) The influence of the Madden-Julian Oscillation activity anomalies on Yunnan's extreme drought of 2009–2010. *Sci China Earth Sci* 55:98–112
- Mahmood R, Babel MS (2014) Future changes in extreme temperature events using the statistical downscaling model (SDSM) in the trans-boundary region of the Jhelum river basin. *Weather Clim Extremes* 5–6:56–66
- Mahmood R, Babel MS, Jia S (2015) Assessment of temporal and spatial changes of future climate in the Jhelum river basin, Pakistan and India. *Weather Clim Extremes* 4:40–55
- Marengo JA, Jones R, Alves LM, Valverde MC (2009) Future change of temperature and precipitation extremes in South America as derived from the PRECIS regional climate modeling system. *Int J Climatol* 29:2241–2255
- Mason SJ, Waylen PR, Mimmack GM, Rajaratnam B, Harrison JM (1999) Changes in extreme rainfall events in South Africa. *Clim Change* 41:249–257
- Mesweeney CF, Jones RG, Booth BBB (2012) Selecting ensemble members to provide regional climate change information. *J Clim* 25:7100–7121
- Meinshausen M, Meinshausen N, Hare W, Raper SCB, Frieler K, Knutti R, Frame DJ, Allen MR (2009) Greenhouse-gas emission targets for limiting global warming to 2|[thin]||[deg]C. *Nature* 458:1158–1162
- Moriyas DN, Arnold JG, Van Liew MW, Bingner RL, Harmel RD, Veith TL (2007) Model evaluation guidelines for systematic quantification of accuracy in watershed simulations. *Trans Asabe* 50:885–900
- Murphy JM, Sexton DM, Barnett DN, Jones GS, Webb MJ, Collins M, Stainforth DA (2004) Quantification of modelling uncertainties in a large ensemble of climate change simulations. *Nature* 430:768–772
- Murphy JM, Sexton DMH, Jenkins GJ, Boorman PM, Booth BBB, Brown CC, Clark RT, Collins M, Harris GR, Kendon EJ (2009) UK climate projections science report: climate change projections
- Noguer M, Jones RG, Hassell DC, Hudson DA, Wilson SS, Jenkins GJ, Mitchell JFB (2003) Workbook on generating high resolution climate change scenarios using PRECIS
- Panthou G, Vischel T, Lebel T, Blanchet J, Quantin G, Ali A (2012) Extreme rainfall in West Africa: a regional modeling. *Water Resour Res* 48:682–688
- Pepler AS, Díaz LB, Prodhomme C, Doblas-Reyes FJ, Kumar A (2015) The ability of a multi-model seasonal forecasting ensemble to forecast the frequency of warm, cold and wet extremes. *Weather Clim Extremes* 7:68–77
- Programme UCI (2009) UK climate projections (UKCP09)
- Qin N, Wang J, Yang G, Chen X, Liang H, Zhang J (2015) Spatial and temporal variations of extreme precipitation and temperature events for the Southwest China in 1960–2009. *Geoenviron Disasters* 2:1–14
- Qiu J (2010) China drought highlights future climate threats. *Nature* 465:142–143
- Root TL, Price JT, Hall KR, Schneider SH, Rosenzweig C, Pounds JA (2003) Fingerprints of global warming on wild animals and plants. *Nature* 421:57–60
- Salmi T, Määttä A, Anttila P, Ruoho-Airola T, Amnell T, Salmi T, Määttä A, Amnell T (2002) Detecting Trends of Annual Values of Atmospheric Pollutants by the Mann-Kendall Test and Sen's Solpe Estimates the Excel Template Application MAKESENS. *Universitas Gadjah Mada* 31
- Sang YF, Wang Z, Liu C (2014) Comparison of the MK test and EMD method for trend identification in hydrological time series. *J Hydrol* 510:293–298
- Schoof JT, Robeson SM (2015) Projecting changes in regional temperature and precipitation extremes in the United States. *Weather Clim Extremes* 11:28–40
- Sun W, Mu X, Song X, Wu D, Cheng A, Qiu B (2016) Changes in extreme temperature and precipitation events in the Loess Plateau (China) during 1960–2013 under global warming. *Atmos Res* 168:33–48
- Timbal B, Jones DA (2008) Future projections of winter rainfall in southeast Australia using a statistical downscaling technique. *Clim Change* 86:165–187
- Torma C, Giorgi F, Coppola E (2015) Added value of regional climate modeling over areas characterized by complex terrain—precipitation over the Alps. *J Geophys Res Atmos* 120:3957–3972
- Wang X, Huang G, Lin Q, Nie X, Cheng G, Fan Y, Li Z, Yao Y, Suo M (2013) A stepwise cluster analysis approach for downscaled climate projection—a Canadian case study. *Environ Model Softw* 49:141–151
- Wang X, Huang G, Liu J (2014) Projected increases in near-surface air temperature over Ontario, Canada: a regional climate modeling approach. *Clim Dyn* 45:1381–1393
- Wang X, Huang G, Lin Q, Nie X, Liu J (2015a) High-resolution temperature and precipitation projections over Ontario, Canada: a coupled dynamical-statistical approach. *Q J R Meteorol Soc* 141:469–472
- Wang X, G. Huang J, Liu, Z. Li, Zhao S (2015b) Ensemble Projections of regional climatic changes over Ontario, Canada. *J Clim* 28:7327–7346
- Wang L, Wu Z, Wang F, Du H, Zong S (2016) Comparative analysis of the extreme temperature event change over Northeast China and Hokkaido, Japan from 1951 to 2011. *Theor Appl Climatol* 124:1–10
- Yu E, Sun J, Chen H, Xiang W (2014) Evaluation of a high-resolution historical simulation over China: climatology and extremes. *Clim Dyn* 45:1–19
- Zhang Q, Li J, David Chen Y, Chen X (2011) Observed changes of temperature extremes during 1960–2005 in China: natural or human-induced variations? *Theor Appl Climatol* 106:417–431
- Zhang Q, Xiao M, Singh VP, Wang Y (2016a) Spatiotemporal variations of temperature and precipitation extremes in the Poyang Lake basin, China. *Theor Appl Climatol* 124:855–864
- Zhang S, Tao F, Zhang Z (2016b) Changes in extreme temperatures and their impacts on rice yields in southern China from 1981 to 2009. *Field Crops Res* 189:43–50
- Zhang Y, Huang G, Wang X, Liu Z (2017) Observed changes in temperature extremes for the Beijing–Tianjin–Hebei region of China. *Meteorol Appl* 24:74–83
- Zhou B, Wen QH, Xu Y, Song L, Zhang X (2014) Projected changes in temperature and precipitation extremes in China by the CMIP5 multimodel ensembles. *J Clim* 27:6591–6611